Mountainous Floodplain Connectivity in Response to Hydrological Transitions

Tristan Babey, Zach Perzan, Sam Pierce, Brian Rogers, Lijing Wang, Rosemary W. H. Carroll, John R Bargar, Kristin Boye, Kate Maher

Water Resources Research

RESEARCH ARTICLE
10.1029/2024WR037162

Mountainous Floodplain Connectivity in Response to Hydrological Transitions

Tristan Babey[1,2], Zach Perzan[1], Sam Pierce[3], Brian Rogers[1], Lijing Wang[4], Rosemary W. H. Carroll[5], John R. Bargar[6], Kristin Boye[3], and Kate Maher[1]

[1]Department of Earth System Science, Stanford University, Stanford, CA, USA, [2]Géosciences Rennes, Université de Rennes, Rennes, France, [3]Stanford Synchrotron Radiation Lightsource, SLAC National Accelerator Laboratory, Menlo Park, CA, USA, [4]Earth and Environmental Sciences Area, Lawrence Berkeley National Laboratory, Berkeley, CA, USA, [5]Desert Research Institute, Reno, NV, USA, [6]Pacific Northwest National Laboratory, Richland, WA, USA

Key Points:

- Soil / gravel bed connectivity in floodplains is important for water quality
- Snowmelt and drought both reduce soil / gravel bed connectivity
- Beaver ponding increases downward flushing to gravel bed unit

Supporting Information:

Supporting Information may be found in the online version of this article.

Correspondence to:

T. Babey,
tristan.babey@univ-rennes.fr

Citation:

Babey, T., Perzan, Z., Pierce, S., Rogers, B., Wang, L., Carroll, R. W. H., et al. (2024). Mountainous floodplain connectivity in response to hydrological transitions. *Water Resources Research*, *60*, e2024WR037162. https://doi.org/10.1029/2024WR037162

Received 18 JAN 2024
Accepted 10 JUN 2024

Abstract In mountainous watersheds, floodplain sediments are typically characterized by gravel bed layers capped by an overlying soil unit that serves as a hotspot for biogeochemical reactivity. However, the influence of soil biogeochemistry on gravel bed underflow composition remains unclear, especially during hydrological transitions that alter the vertical connectivity between overlaying soils and the underlying gravel bed. This study investigates these dynamics by measuring hydraulic gradients and water compositions over three hydrological years in a typical mountainous, low-order stream floodplain in the Upper Colorado River Basin. Results indicate that the timing of hydrological conditions strongly influences the vertical exchanges that control water quality. Specifically, during flooding events such as beaver ponding, that induce downward flushing of the soil, anoxic conditions prevalent in the biogeochemically active soil are transferred downstream via gravel bed underflow. Conversely, snowmelt and drought conditions increase oxic conditions in the gravel bed due to diminished hydrological connectivity with the overlying soil. To compare water quality response to hydrological transitions across similar floodplain environments, we propose a conceptual model that quantifies the inundation-induced flushing of soil porewater to measure solute exchange efficiency with the gravel bed solute convergence efficiency (SCE). This model provides a framework for quantifying biogeochemical processes in hydrological underflow systems, which is critical for water and elemental budgets in these globally important mountainous ecosystems.

Plain Language Summary Mountains are important sources of freshwater for humans and ecosystems. They are however increasingly impacted by climate change. In this paper, we investigate how changes in water availability (droughts, snowmelt, inundations) can cascade into changes in water quality (concentrations of dissolved chemical elements). We show that in mountain valleys, the zone of contact between the soil and the underlying gravel bed aquifer is important for water quality. Chemical elements from the soil can be flushed down into the gravel bed aquifer, then transported by groundwater to the stream. Chemical elements from the soil can also react with chemical elements present in the aquifer. Our research can be used to better predict the water and elemental budgets in these important mountainous systems.

1. Introduction

Mountainous gravel-bed river floodplains are important ecosystems that moderate groundwater and surface water exchanges (Hauer et al., 2016; Käser & Hunkeler, 2016; Miller et al., 2016; Rumsey et al., 2015). Gravel-bed river floodplains develop in the broader sections of mountain valleys filled with unconsolidated, high permeability alluvial or glacial sediments (Hauer et al., 2016; Stanford & Ward, 1993). Because of their strong connection to surface waters and relatively fast groundwater flow (10–100 s of cm/day), gravel bed aquifers tend to remain oxic, especially during snowmelt periods that induce large influx of oxygenated water (Noël et al., 2017; Yabusaki et al., 2017). In contrast to the underlying gravel bed, overlying riparian soils are intensely biogeochemically active, often exhibiting anoxia when water saturated (Dewey et al., 2021; Tolar et al., 2020). Soil/gravel bed contacts commonly span tens of square kilometers at the watershed scale in inter-mountain valleys and thus have the potential to strongly influence water quality. Yet, to date, no studies have mechanistically linked hydro-biogeochemical activity in redox-active riparian soils to groundwater dynamics in underlying gravel-cobble alluvium.

Gravel-bed floodplains are also increasingly impacted by climate change through snowpack reduction, earlier snowmelt, and the intensification of droughts (Clow, 2010; Hidalgo et al., 2009; Meixner et al., 2016; Udall & Overpeck, 2017). Hydrological perturbations that modify biogeochemical cycles can further impact water quality, putting additional pressure on already threatened water resources (Mishra et al., 2021). The latter can occur when falling water tables, driven by increasing aridity, enhance chemical weathering and increase metal and sulfate loading in natural waters during subsequent infiltration events (Manning et al., 2013; Todd et al., 2012). Extreme rainfall and flooding events, which are also increasing globally, can lead to periods of prolonged saturation and/or enhanced connectivity between floodplains and surface waters that alter biogeochemical cycles (Ascott et al., 2016; Scott et al., 2014; Yang et al., 2023).

Hydrological perturbations that change the direction or intensity of groundwater flow may also alter the biogeochemical reactions. For example, a large influx of dissolved oxygen into anoxic sediments can overcome their redox buffering capacity and their ability to reduce redox-sensitive contaminants (Pan et al., 2018; Perzan et al., 2021; Yabusaki et al., 2017). On the one hand, groundwater routing through hydro-biogeochemical interfaces has been identified as a primary control of the mobilization or attenuation of nutrients and contaminants at the sub-meter scale (for example, Aeppli et al., 2022; Babey et al., 2022; Engel et al., 2021; Janot et al., 2016; Kumar et al., 2020; Noël et al., 2017). On the other hand, the maintenance of strong biogeochemical gradients is often contingent on the rate of solute and water exchanges across these interfaces, which may restrict their impact on overall groundwater composition. Although hyporheic zone studies have highlighted the dynamics of exchanges during hydrological transitions (for example, Voltz et al., 2013; Ward et al., 2016), and the importance of lithologic and geomorphic controls on scaling of these exchanges (for example, Allgeier et al., 2021; Cardenas, 2009; Wang et al., 2018), the attendant vertical exchanges between heterogeneous sediment layers typical of alluvial floodplains have not been examined. However, these exchange flows have the potential to drive impactful biogeochemical hotspot activity.

In this paper, we monitored water and solute transfers across a soil/gravel bed interface located in the Upper Colorado River Basin. Over 3 years of measurements, the floodplain was subjected to marked hydrological shifts, including snowmelt, summer droughts and the periodic filling and draining of an adjacent beaver pond. Our goals were: (a) to quantify the spatiotemporal variability of soil/gravel bed exchanges across the floodplain and across hydrological transitions; (b) to identify the main geomorphological, hydrological, and biogeochemical drivers of this variability; and (c) to assess the contribution of floodplain soil/gravel bed interfacial dynamics to water quality, ultimately of relevance at watershed scale.

2. Methods

2.1. Site Description

This study was conducted at a riparian floodplain (~3,600 m^2, Figure 1) adjacent to the Slate River, immediately downstream of the confluence of Oh-Be-Joyful (OBJ) Creek and Slate River, in the Upper Colorado River Basin, USA (38°54′34.59″ N, 107°1′43.40″ W). This OBJ site is located 1.6 km northwest of Crested Butte, CO. The Slate River watershed is a mountainous, high-elevation catchment (2,700–3,400 masl) where hydrology is dominated by snowmelt dynamics. Average precipitation over the 2020–2022 period were estimated at 877 mm/y (34% as snow) with monthly mean temperatures ranging from −14°C (January) to 13°C (July) (Global Historical Climatology Network (GHCN) and SNOpack TELemetry (SNOTEL) sites of Crested Butte (USC00051959)). Slate River discharge peaks in late May/early June during snowmelt (~20 m^3/s, Figure 2) then recedes over the summer to reach baseflow by the end of August (~0.2 m^3/s). Estimated Strahler stream order is three, corresponding to a drainage area of 73 km^2. Geophysical and geological surveys indicate that the OBJ floodplain is comprised of 1–3 m of soil over approximately 10 m of unconsolidated gravel and cobble alluvium ("gravel bed" in the following), underlain by Cretaceous to Tertiary sedimentary Mancos Shale bedrock (Gaskill et al., 1967; Kimball et al., 2010). The riparian soil is heterogeneous and constituted of interspersed sandy, silty and clayey layers, with occasional thin (<5 cm) layers of medium gravel (Figure S1 in Supporting Information S1). Floodplain vegetation is dominated by grasses and several willow species (Salix spp.). Peak vegetative greenness occurs seasonally around the third week of July. The floodplain topography is characterized by an 80-m-long northern border with a seasonally filling and draining beaver pond, a 150-m-long western and southern border with coniferous evergreen forest, a 50-m-long eastern border with a deep (1.5 m) beaver-built diversion channel,

10.1029/2024WR037162

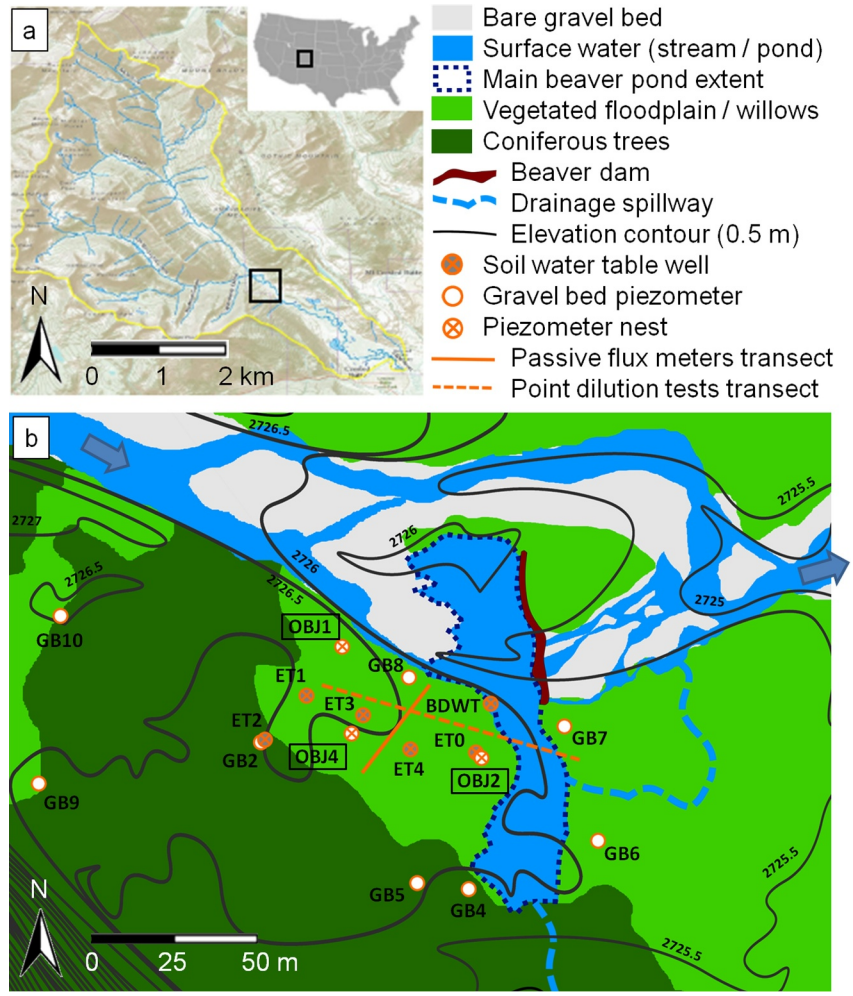

Figure 1. (a): Location and overview map of the Upper Slate River watershed, with watershed boundaries indicated in yellow (Bembenek, 2014) (b): map of the SLAC-SFA Slate River experimental site derived from airborne LIDAR data and drone imagery, including well network detail. The extent of the stream and the beaver pond is representative of baseflow hydrological conditions. Flow in the stream is from top left to top right.

and a network of scattered shallow beaver-built channels across the eastern half. The average down-valley topographical gradient of the floodplain is 0.8%.

Following the instrumentation of the OBJ site during Summer 2019, this site has experienced significant hydrological perturbations due to the unexpected construction in September 2019 of a channel-spanning beaver dam across the southern braid of the Slate River bordering the northern edge of the floodplain (Figure 1). As of May 2023, the dam has been continuously maintained by beavers and has resisted breaching during spring runoff since its initial construction. Perturbations from the dam include a sustained rise in water table elevation across the floodplain during spring runoff, seasonal surface flooding across the eastern portion of the floodplain, rapid draining of ponded areas as river stage drops, and episodic flooding and draining events. In September 2021, December 2021 and July–October 2022, the beaver pond was completely dry and void of surface flow (Figure 2). As precipitation and stream discharge were roughly equivalent over the 2020–2022 period, the draining of the pond likely resulted from the deposition of a gravel bar upstream of the OBJ site during spring 2021 that redirected more water to the northernmost braid of the river and away from the beaver pond (Figure 1). Several years of damming has resulted in substantial large wood deposition and sedimentation along the dam structure and river channel floor, reaching depths up to 30–50 cm in places.

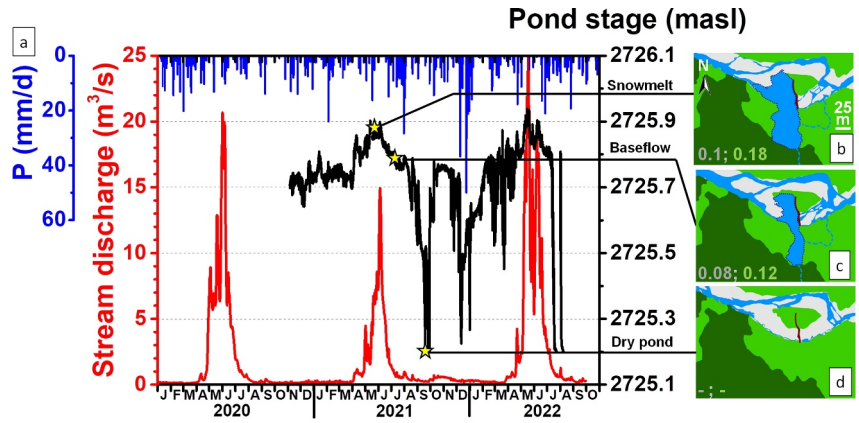

Figure 2. (a): Daily precipitations (excluding snow), mean daily stream discharge and surface water elevation in the beaver pond at the SLAC-SFA OBJ field site over the 2020–2022 period. Slate River stream discharge was measured at the Gunsight Bridge USGS (United States Geological Survey) gauging station (~300 m downstream of the OBJ site) complemented by a seasonal regression on measurements from the Baxter Gulch USGS gauging station (~9 km downstream of the OBJ site) for missing data (January–November 2020 and November 2021–April 2022) (Figure S2 in Supporting Information S1). Pond stage was measured at well BDWT (Figure 1). (b), (c) and (d): Characteristic spatial extent of the beaver pond for snowmelt, baseflow, and dry pond hydrological conditions, respectively. The gray and light green numbers correspond to the flooded surface area (in ha) over the bare gravel riverbed and over the riparian soil, respectively.

2.2. Water Table Monitoring

To monitor water levels throughout the alluvial aquifer system, we installed three types of wells and piezometers across the floodplain: water table wells, gravel bed piezometers and soil piezometers. Water table wells consist of 4 cm diameter PVC pipe screened from 0.1 m below the surface to the soil-gravel interface (1.6—2.35 m depth, depending on the location). Each gravel bed piezometer is constructed from 4-cm diameter steel pipe attached to a shielded piezometer tip with a 15 cm screen length (Solinst Model 615NS). Piezometers completed in the soil consist of 4-cm diameter PVC pipe attached to a PVC piezometer tip with a 15 cm screen length (Solinst Model 601).

In total, we installed five water table wells, nine gravel bed piezometers and six soil piezometers across the floodplain (Figure 1). All gravel bed piezometers were installed at a uniform depth and screened between 3.23 and 3.38 m below the ground surface. To measure the vertical hydraulic gradient within and between each alluvial unit, we also installed nests of vertically stacked soil piezometers alongside gravel bed piezometers. Two piezometer nests (OBJ1 and OBJ2) contain two soil piezometers and one gravel bed piezometer, while the third (OBJ4) contains two soil and two gravel bed piezometers (see Figure S3 in Supporting Information S1 for installations schematics). Within each nest, each piezometer screen is vertically offset by a minimum of 0.6 m. Finally, we installed an additional soil piezometer in the sediment underlying the beaver pond (BDWT). Following installation, well and piezometer elevations were surveyed using a real-time kinematic positioning system (Topcon Hyper-V RTK-GPS) with ~0.015 cm of vertical accuracy. Two piezometers could not be surveyed with the real-time kinematic system and instead were surveyed by measuring elevation differences between each piezometer casing and established points using a reflectorless Total station. The elevation error from this method is estimated at 0.03 m.

All wells and piezometers were instrumented with pressure transducers (Onset HOBO U20L) that recorded hourly pressure and temperature. Because the top of the piezometer casing for BDWT is submerged beneath the beaver pond, the pressure recorded by this transducer reflects water levels in the pond. All other transducers record pressure within the piezometer casing. Water levels were calculated from pressure data by correcting for variations in barometric pressure, using a combination of atmospheric pressure sensors at different time points depending on data availability: a meteorological station (Ambient Weather WS-2902) located 6.5 km to the south (November 2020—May 2021) and a barometric pressure sensor (Campbell Scientific CS100) installed aboveground at site OBJ2 (all other time points). A comparison between these disparate data sources shows that using an atmospheric pressure sensor further away from the site introduces <0.015 m error in final computed water levels. In addition, because this error is constant across all transducers for a given time point, it does not impact

calculated hydraulic gradients. We validated water level data in each well or piezometer by comparing computed water levels with 10–12 manual measurements over the course of the study period.

2.3. Groundwater Velocity

Given the expected difference in groundwater velocities between the soil and the gravel bed, different methods were used to measure flow rates in each unit. Groundwater velocity in the soil was quantified at three locations using passive flux meters (PFMs) from EnviroFlux (Hatfield et al., 2004). For this study, PFMs were installed in three piezometers along a 30-m transect perpendicular to the river (Figure 1), with the center of each PFM between 1.1 and 1.4 m below the ground surface and a minimum of 0.65 m above the soil-gravel interface. PFMs were deployed over 26 days in August 2021, then removed at the end of deployment and destructively sampled to quantify tracer elution. Thus, calculated Darcy velocities (specific discharge) from each PFM represent the average velocity over the screened interval over the length of the 26-day deployment.

Groundwater velocity in the gravel bed was measured by performing point dilution tests using the method of Perzan and Chapin (2023). First, drive-point piezometers were installed in three locations along a transect parallel to the river (Figure 1). Each piezometer used a 15-cm screen length with the center of each screened interval installed 1.1 m below the soil-gravel interface. Inexpensive electrical conductivity sensors known as WellSTICs (Perzan & Chapin, 2023) were then used to perform two point dilution tests in August 2021. During each test, we first established a gas-free loop of re-circulating water between each piezometer screen and the surface. We then injected 30 ml of local groundwater spiked with 1 g NaCl and continued to re-circulate water until electrical conductivity had returned to pre-injection values, which took 1–5 hr depending on the test. The decay in electrical conductivity over time was used to compute the magnitude of the average linear groundwater velocity, assuming a point dilution shape factor of 2.36 (Hoppe, 2013). Complete details of these tests are described by Perzan and Chapin (2023).

2.4. Groundwater Geochemistry Monitoring

Geochemical measurements were realized monthly on average during snow-free periods (May–September) when the OBJ site was accessible, with higher sampling frequency (~weekly) during snowmelt (May–June). Porewater was extracted from fine-grained soil sediments using a network of aluminum rhizon sampling wells (Rhizosphere Research Products, part no. 19.60.21F, 10 cm porous length, 0.6 μm mesh size, modified by replacing original plastic tubing with aluminum tubing to minimize redox changes during sampling). Rhizons were installed vertically at 20 cm intervals spanning the layer of fine-grained sediments to the cobble aquifer interface. Groundwater was extracted from the gravel bed aquifer using stainless steel drive-point piezometric wells (Solinst Canada Ltd., Model 615S, 50 mesh cylindrical filter-screen). Piezometers were installed to depths directly below the cobble interface and up to 2 m into the aquifer. Water intended for in situ measurements of specific conductance, dissolved oxygen and alkalinity was immediately utilized once sufficient volume was extracted. Measurements for specific conductance were taken using a Thermo Scientific Orion DuraProbe 4-Electrode conductivity cell. Dissolved oxygen was measured colorimetrically using a portable V-2000 multi-analyte photometer and CHEMetrics vacu-vials®, and using either the indigo carmine method (#K-7513, 1–15 ppm) for piezometer-extracted cobble water or the Rhodamine D™ method (#K-7553, 0–1 ppm) for rhizon-extracted soil porewater. Alkalinity was measured visually using CHEMetrics Titrets® Kits (#K-9810, 10–100 ppm as $CaCO_3$ and #K-9815, 50–500 ppm as $CaCO_3$).

2.5. Calculation of Hydraulic Parameters

Horizontal hydraulic gradients in the gravel bed and in the soil were calculated using a linear interpolation on triangular planes between all piezometer locations in the gravel bed (GB wells) and in the soil (ET wells) (Figure 1) (Fetter, 1981). The spatial mean and standard deviation of the gradient direction were calculated using the circular statistics toolbox CircStat of MATLAB (Berens, 2009). The horizontal hydraulic conductivity was determined experimentally for the gravel bed and the soil (Section 2.3) and the corresponding horizontal Darcy flow was then determined by using the Darcy equation.

Vertical hydraulic gradients at the soil-gravel bed interface were calculated at three piezometer nests (OBJ1, OBJ2 and OBJ4, Figure 1). For each nest, we used the hydraulic heads measured directly above and below the interface, with screened depths separated by ~1 m (Text S4 in Supporting Information S1). Vertical Darcy flow

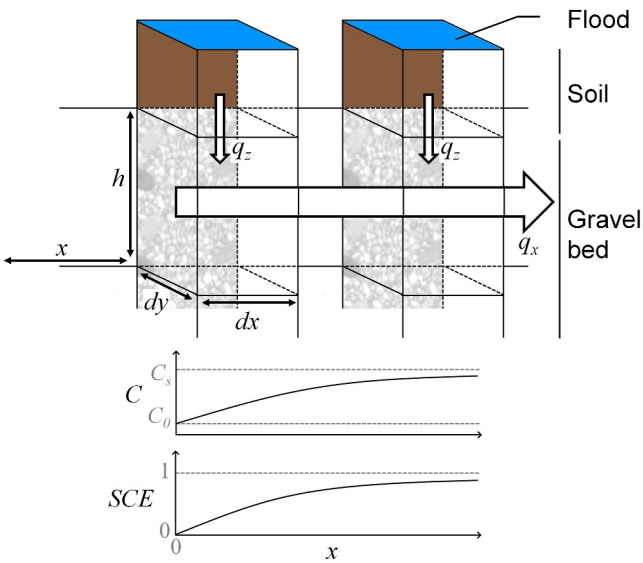

Figure 3. Schematic illustration of the two-dimensional model defined in Section 2.6 in which downward drainage (q_z) from an overlaying inundation leads to the accumulation of soil-originated water and solutes in the gravel bed as a function of the distance x along the flow path denoted by q_x. This accumulation leads to the increase of solute concentrations in the gravel bed C from the initial concentration C_0 toward the soil concentration C_s, and to the increase of the solute convergence efficiency SCE from 0 to 1.

was then calculated by using the Darcy equation and the value of vertical hydraulic conductivity for the soil determined by using the analytical model of Section 2.6. The calculated horizontal and vertical hydraulic conductivities were then considered as homogeneous across their respective sedimentary units in the floodplain. Finally, we calculated the Peclet number $Pe = q_z\lambda/D_e$, where q_z is the vertical Darcy flow, λ is the characteristic transport distance taken equal to 10 cm (i.e., comparable to the vertical distance between consecutive sampling points for geochemical measurements), and $D_e = 1.0 \times 10^{-5}$ cm^2/s is the effective diffusion coefficient selected from the literature for similar floodplain environments (Arora et al., 2016; Babey et al., 2022), which corresponds to half the self-diffusion coefficient of Cl^- at infinite dilution in pure water (Lide, 2004).

2.6. Analytical Solution for Solute Accumulation in the Gravel Bed

We developed 1D reactive transport calculations to evaluate the accumulation of solutes in the gravel bed resulting from vertical drainage from the soil. The gravel bed was approximated as a plug-flow reactor undergoing continuous interfacial mass transfers from the overlaying soil and into the deeper parts of the aquifer (Figure 3). This analytical model was obtained by modifying the plug-flow reactor model presented by Nazaroff and Alvarez-Cohen (2001) to account for vertical mass transfers driven by advection rather than diffusion. At steady state, the solute mass balance in the gravel bed is given by:

$$q_x h dy[C(x) - C(x+dx)] + q_z dx\, dy[C_s - C(x)] + r h dy\, dx = 0 \quad (1)$$

where x is the position along the horizontal flow direction in the gravel bed; C is the solute concentration in the gravel bed, assumed to be homogeneous over the mixing height h; C_s is the solute concentration in the overlaying soil; q_x and q_z are the horizontal and vertical Darcy flow velocities; and r is the solute reaction rate. Assuming that the solute undergoes a first-order irreversible degradation in the gravel bed $r = -kC$, where k is the degradation constant, Equation 1 can be re-written as:

$$\frac{dC(x)}{dx} = -\frac{q_z + hk}{q_x h}C(x) + \frac{q_z}{q_x h}C_s. \quad (2)$$

The concentration gradient in the gravel bed is thus determined by the balance between solute removal rate by dilution and degradation $\frac{q_z+hk}{q_x h}C(x)$, and solute transfer rate from the overlying soil $\frac{q_z}{q_x h}C_s$. Posing $C(x=0) = C_0$, this equation is integrated along the cross-section of the floodplain aquifer in the x direction:

$$C(x) = \left(C_0 - \frac{q_z}{q_z + hk}C_s\right) \times \exp\left(-\frac{q_z + hk}{q_x h}x\right) + \frac{q_z}{q_z + hk}C_s. \quad (3)$$

In the case of a conservative solute ($k = 0$), Equation 3 rewrites:

$$C(x) = (C_0 - C_s) \times \exp\left(-\frac{q_z}{q_x h}x\right) + C_s \quad (4)$$

where $q_z x$ corresponds to the cumulative downward flow from the soil over the travel distance x and $q_x h$ corresponds to the cumulative horizontal flow in the gravel bed over the height h. The exponential term thus corresponds to the fraction of soil-originated water accumulated in the gravel bed at a position x along the horizontal flow path:

$$f_{SW} = \frac{q_z x}{q_x h}. \quad (5)$$

In the case of a reactive solute ($k > 0$) initially present in the gravel bed but with negligible concentration in the soil layer ($C_s = 0$), such as dissolved oxygen, Equation 3 is expressed as:

$$C(x) = C_0 \times \exp\left(-\frac{q_z + hk}{q_x h}x\right) \tag{6}$$

We note that in this latter case, solute concentrations in the gravel bed decrease exponentially along x according to the apparent degradation constant $\frac{q_z+hk}{q_x h}$ that incorporates the effects of both dilution due to mixing and of biogeochemical reactivity.

Finally, we define the solute convergence efficiency (SCE) to characterize how concentrations in the gravel bed converge toward concentrations in the soil due to the accumulation of downward transfers:

$$SCE = \frac{C(x) - C_0}{C_s - C_0}. \tag{7}$$

The SCE thus correspond to a metric for evaluating the efficiency of solute exchange between the soil and the gravel bed, ranging from 0 ($C(x) = C_0$) to 1 ($C(x) = C_s$). In the case of a conservative solute, the SCE can be directly calculated as a function of f_{SW} by rearranging Equation 4:

$$\frac{C(x) - C_0}{C_s - C_0} = 1 - \exp\left(-\frac{q_z}{q_x h}x\right). \tag{8}$$

3. Results

3.1. Horizontal Flow Dynamics

Horizontal hydraulic gradients in the gravel bed remained, on average, aligned with the topographic down-valley gradient over the 2020–2022 period, both in terms of magnitude (~0.8%, Figure 4a) and direction (NW to SE, Figure 4b). During snowmelt periods (April–June), this magnitude decreased by 30% while groundwater flow rotated toward the stream down-valley direction (W to E). Lower hydraulic gradients during snowmelt were consistent with the floodplain becoming waterlogged, with more limited water drainage. Gradient alignment with the stream down-valley direction would express the increased influence of the stream boundary condition during peak stream discharge, which was two orders of magnitude larger than during baseflow (15 and 0.3 m^3/s respectively, Figure 2). Groundwater flow rates in the gravel bed also showed no response to water level variations in the beaver pond, even when the pond was dry (Figure 2).

In contrast, horizontal hydraulic gradients in the soil responded strongly to hydrological shifts, and in particular, to the presence of the beaver pond. During baseflow, lateral recharge of the floodplain by the beaver pond (NE to SW, cross-valley direction) resulted in horizontal hydraulic gradients in the soil becoming perpendicular to gradients in the underlying gravel bed (Figure 4b). During snowmelt, horizontal hydraulic gradients in the soil tended to rotate toward the down-valley direction, while their amplitude decreased as the floodplain became waterlogged. Finally, when the pond dried out (summer 2021, winter 2021, summer 2022), horizontal hydraulic gradients in the soil also rotated toward the down-valley direction, and even slightly toward the valley center (SW to NE) during the extended dry pond period of summer 2022, suggesting that groundwater discharge was supporting stream baseflow. While the magnitude of horizontal hydraulic gradients were similar in the gravel bed and in the soil (~0.8%, Figure 4a), flow rates were two orders of magnitude larger in the gravel bed than in the soil (~150 cm/d and 1 cm/d respectively, Figure 4a), due to the much larger hydraulic conductivity of the gravel bed (2.0×10^{-3} m/s vs. 1.4×10^{-5} m/s for the soil, Table 1).

3.2. Vertical Flow Dynamics at the Soil/Gravel Bed Interface

We used three piezometer nests located at increasing distance from the beaver pond to measure vertical hydraulic gradients at the soil-gravel bed interface across the floodplain. Time series of hydraulic gradients were then converted to vertical flow rates using Darcy's law and the value of vertical hydraulic conductivity for the soil (Table 1).

10.1029/2024WR037162

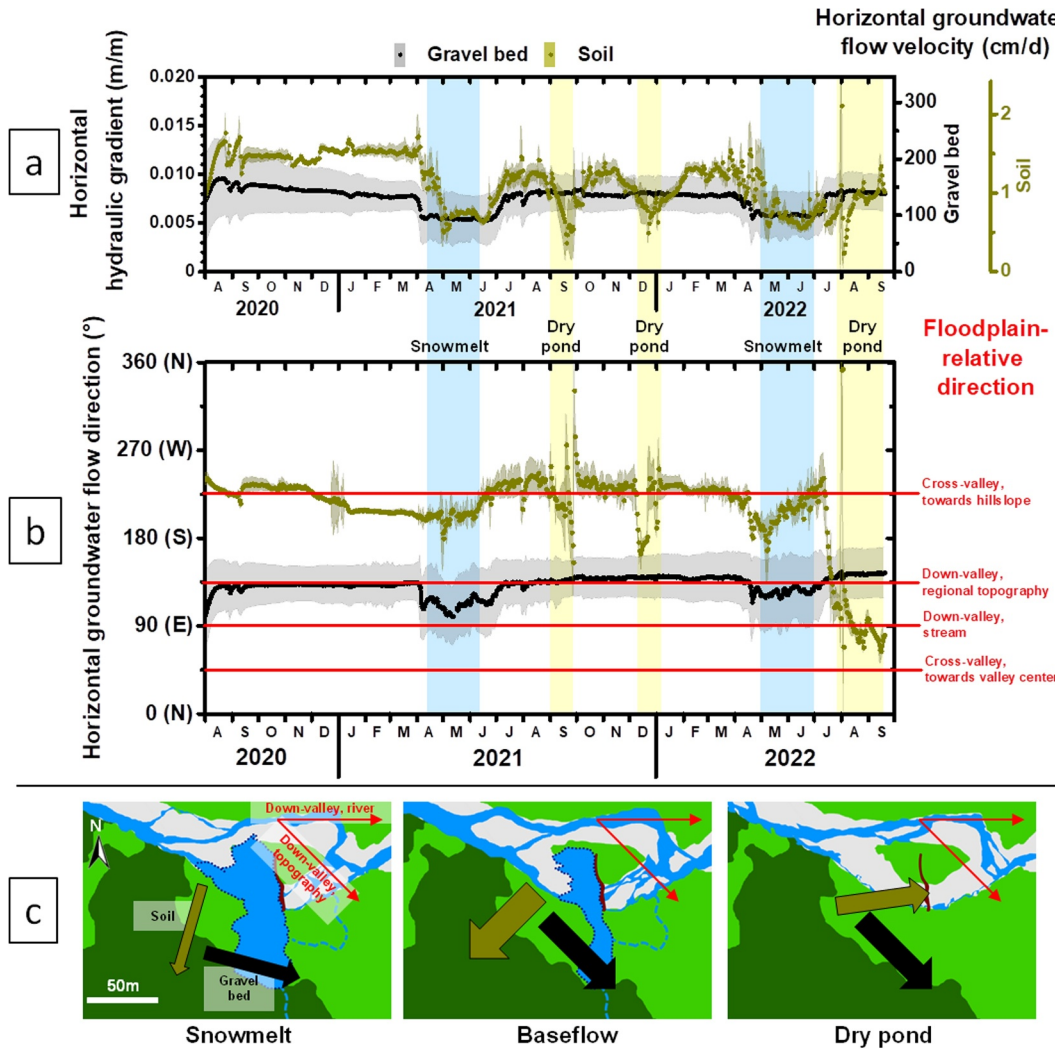

Figure 4. (a): Daily average magnitude and standard deviation of the horizontal hydraulic gradient measured in the soil and in the gravel bed, with corresponding estimations of groundwater flow velocity. (b): Daily average direction of the horizontal hydraulic gradient measured in the soil and in the gravel bed, in relation to significant directions of the floodplain geomorphology. (c): Comparison of the horizontal hydraulic gradient measured in the soil (brown arrow) and in the gravel bed (black arrow) averaged over all snowmelt, baseflow and dry pond periods. Arrow thickness is proportional to the magnitude of the gradient. The direction of the topographic down-valley gradient and of the stream are represented by red arrows.

Table 1
Hydraulic Parameters for the Gravel Bed and the Soil Measured or Calculated at the OBJ Site in August 2021

	q (cm/d)	∇H[a] (−)	K[b] (m/s)
Gravel bed, horizontal direction	174[c]	0.01	2.0×10^{-3}
Soil, horizontal direction	1.22[d]	0.01	1.4×10^{-5}
Soil, vertical direction	4.1[e]	0.3	1.6×10^{-6}

Note. q is the Darcy flow, ∇H is the hydraulic gradient and K is the hydraulic conductivity. [a]Average hydraulic gradient measured at well OBJ2. [b]Calculated using the Darcy equation $q = K\nabla H$. [c]Measured using the point dilution method. [d]Measured using the PFM method. [e]Calculated using the measured accumulation of specific conductance in the gravel bed between wells OBJ1 and OBJ2 (Section 3.4).

Overall, the presence of the beaver pond enhanced downward groundwater flow through the soil/gravel bed interface, with a more pronounced effect near the pond (Figure 5). Proximity to the pond also increased the temporal variability of vertical flow rates, which ranged from $-6 \leq q_z \leq 2$ cm/d near the pond (well OBJ2, negative values indicate downward flow) to $-1 \leq q_z \leq 1$ cm/d at a distance of ∼50 m upstream of the pond (well OBJ1). Comparison of hydraulic heads measured across the floodplain suggest that this variability was likely driven by water level differences between the gravel bed and the pond, as hydraulic heads in the soil remained intermediary between heads in the gravel bed and in the pond (Figure 6). During baseflow, vertical flow rates trended downwards (Figure 5) due to high water levels in the pond and low hydraulic heads in the gravel bed (Figure 6). During snowmelt, quickly rising hydraulic heads in the gravel bed (Figure 6) led to

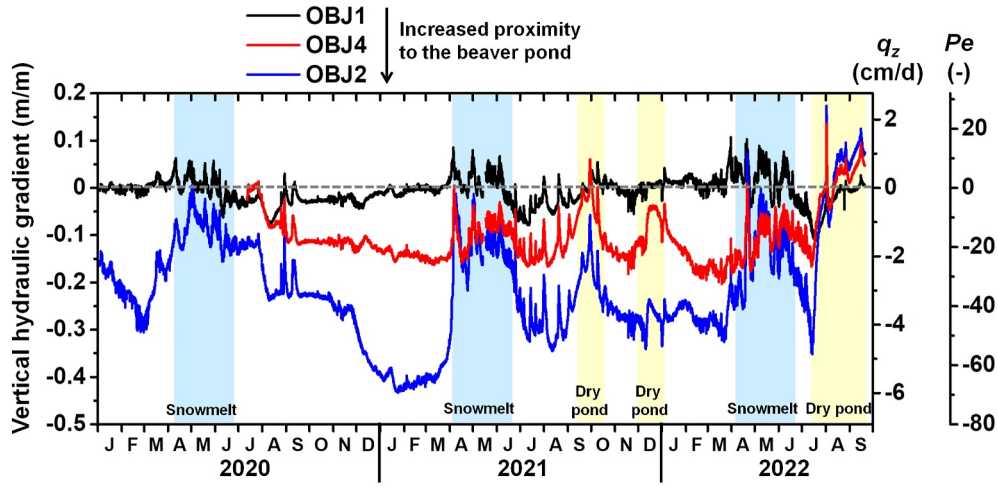

Figure 5. Vertical hydraulic gradient, Darcy flow q_z and Peclet number Pe at the soil-gravel bed interface for the three piezometer nests of the OBJ site. Note that these three variables are linearly related (Section 2.5) and correspond to a change of y-axis scale. Negative values indicate downward flow direction.

the floodplain becoming waterlogged and to more limited vertical flow dynamics (Figure 5). When the pond dried out during summers 2021 and 2022, vertical water exchanges turned upward across the majority of the floodplain (up to ∼ 1 cm/d, Figure 5), presumably driven by a combination of groundwater discharge into the stream (Figure 4) and evapotranspiration. This reversal of vertical flow direction was not observed over the same time period (July–September) in 2020 when the beaver pond was present, highlighting the role of the pond as a driver of downward recharge of the floodplain.

3.3. Dissolved Oxygen, Alkalinity and Specific Conductance Dynamics

Soil profiles at the OBJ site were characterized by the presence of two main oxic-anoxic transitions. The shallowest transition developed over the top ∼1 m of the soil between the zone in contact with the atmosphere and underlying fine-grained, reduced soil horizons (DO ≤ 1 mg/L, Figure 7). The second transition occurred between the anoxic soil and the oxic underlying gravel bed (2 ≤ DO ≤ 8 mg/L) at depths comprised between 150 and 250 cm. Anoxic conditions in the fine-grained soil horizons were associated with higher specific conductance (∼220 µS/cm, Figure 8) and alkalinity (∼120 mg/L, Figure 9). Oxic conditions at the top of the soil profile and in the gravel bed were associated with lower specific conductance (∼75 µS/cm) and lower alkalinity (∼20 mg/L), closer to values measured in the stream (∼70 µS/cm and 18 mg/L respectively, Figures 8 and 9). Despite the similarities in their composition, oxic groundwater at the top of the soil profile and in the gravel bed had different origins, as indicated by the direction of horizontal hydraulic gradients (Figure 4). Groundwater at the top of the soil profile likely corresponded to a mix of infiltrated precipitation and surface water recharged laterally from the nearby beaver pond (<50 m). Oxic groundwater in the gravel bed appeared to be recharged upstream of the floodplain (potentially from the confluence of Slate River and Oh-Be-Joyful Creek, ∼125 m upstream of the site (Figure 1)) before circulating under the soil in the topographic down-valley direction.

The depths of the two main oxic-anoxic transitions evolved with hydrological shifts, which also impacted solute exchanges between the soil and the gravel bed. In the soil, DO concentrations were slightly larger on average in 2020 compared to 2021 (∼2 vs. 0.5 mg/L over the May–September period at OBJ1, Figure 7) together with lower specific conductance (∼180 vs. 210 µS/cm, Figure 8) and lower alkalinity (∼80 vs. 115 mg/L, Figure 9). This was likely due to larger downward flow rates in 2020 compared to 2021 (−2.9 cm/d vs. −2.0 cm/d on average over the May–September period at OBJ2, Figure 5), driving more oxic surface water into the deeper parts of the soil. Larger downward flow rates at the soil-gravel bed interface would also explain the more reducing conditions detected in the gravel bed in 2020 compared to 2021. In 2020, a plume characterized by low DO concentrations (∼1 mg/L, Figure 7), high specific conductance (∼150 µS/cm, Figure 8) and high alkalinity (∼60 mg/L, Figure 9) developed in the gravel bed down to ∼ 2 m under the interface with the soil. This plume only penetrated the first 30 cm under the interface in 2021, as more limited downward flow rates drove less reduced porewater from the

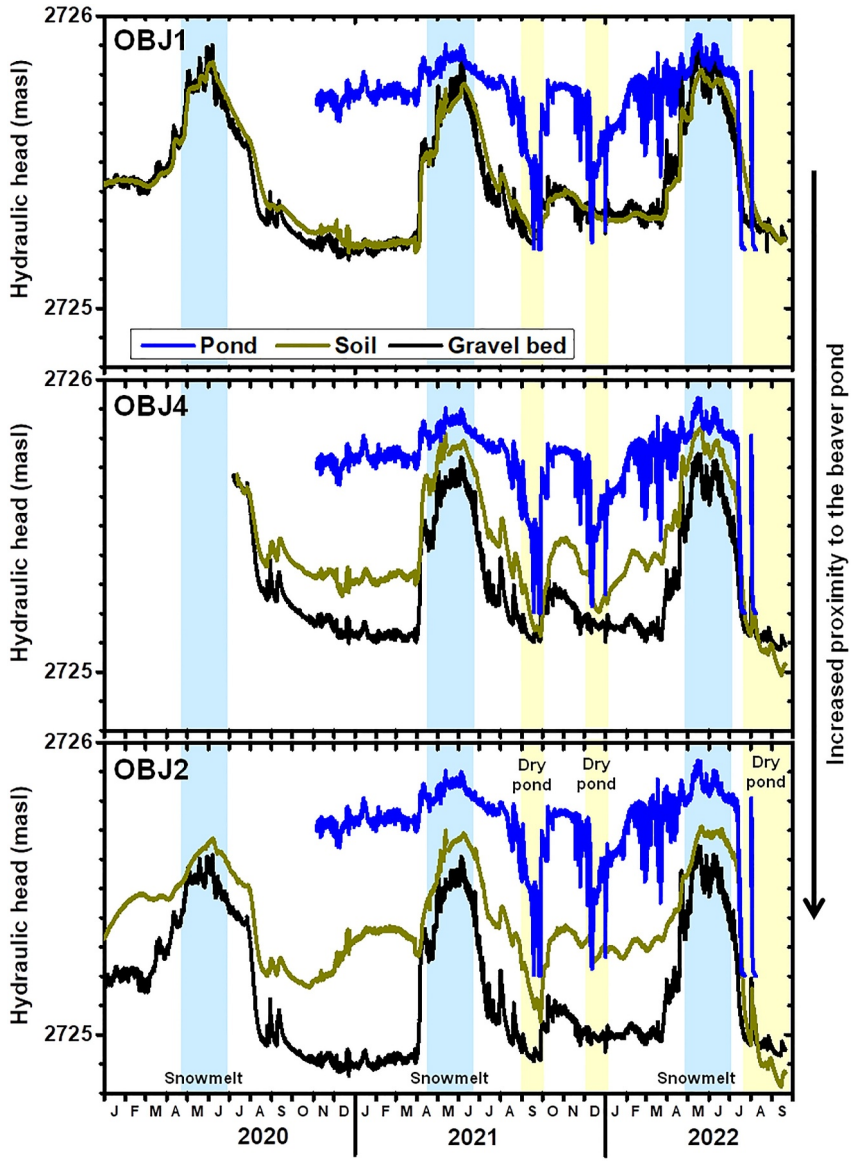

Figure 6. Hydraulic heads measured in the beaver pond, the soil, and the gravel bed for the three piezometer nests of the OBJ site.

soil into the gravel bed. Similar correlations between increased downward flow rates from the soil and increased propagation of reducing conditions into the gravel bed can be identified at the seasonal timescale. Reducing conditions in the gravel bed were the most pronounced during baseflow, when vertical drainage from the soil into the gravel bed was the most important (Figure 5). In contrast, the gravel bed was more oxic during snowmelt (April–June) or during dried pond events (late summer 2021), when vertical exchanges between the soil and the gravel bed became more limited. Peclet number calculations further emphasize the control of vertical flow rates on solute exchanges, as transport across the soil/gravel bed interface was dominated by advection even during low-flow periods (|Pel ≫ 1, Figure 5).

Finally, reducing conditions from the soil propagated deeper as travel distances in the gravel bed under the floodplain increased. In 2021, average DO concentrations within the top 2 m of the gravel bed decreased from 4.2 to 1.9 mg/L between wells OBJ1 and OBJ2 (Figure 7), with OBJ1 located 50 m upstream of OBJ2 (Figure 4). This decrease corresponded to a deeper penetration of reducing conditions (DO < 1 mg/L) below the soil/gravel bed interface, from 60 cm at OBJ1 to 200 cm at OBJ2. Conversely, specific conductance in the top section of the

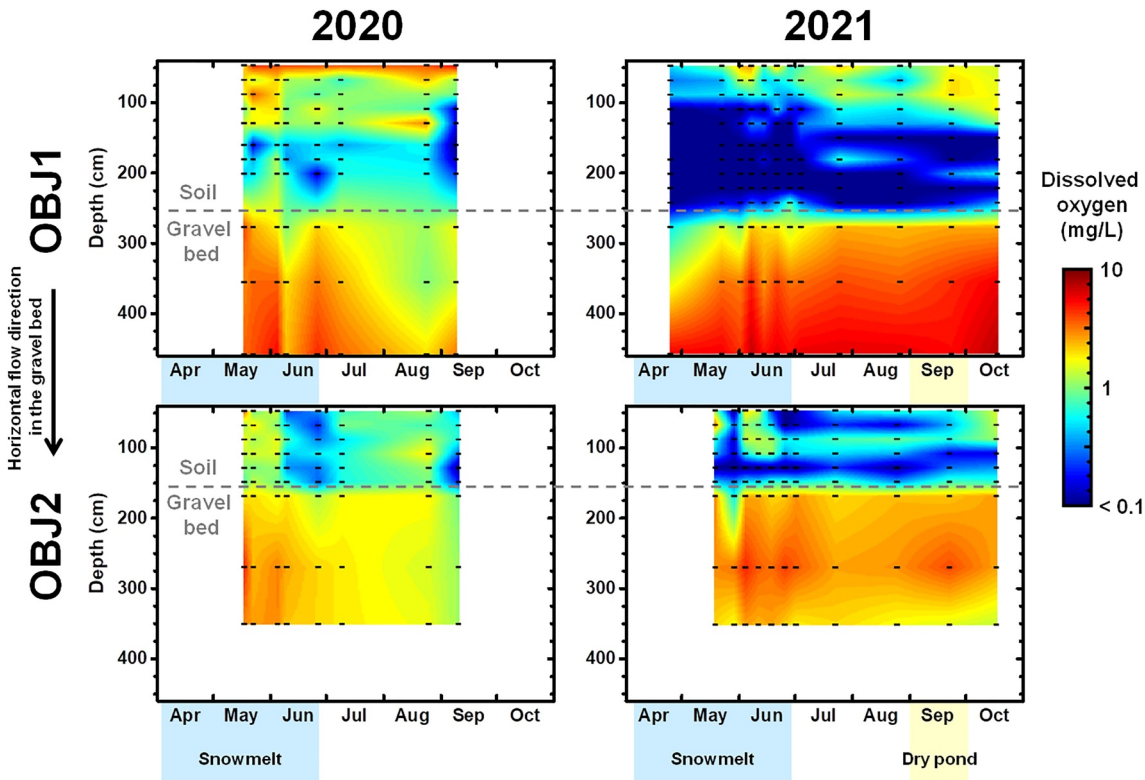

Figure 7. Depth profiles of measured dissolved oxygen concentrations in 2020 (left) and 2021 (right) at wells OBJ1 (top) and OBJ2 (bottom). Color contours are based on linear interpolation between concentration measurements denoted by black dots for depth and date. The depth of the soil-gravel bed interface is indicated by the dashed gray line.

gravel bed increased between OBJ1 and OBJ2 (130 vs. 185 μS/cm, Figure 8) together with alkalinity (40–75 mg/L, Figure 9), approaching conditions prevalent in the overlaying anoxic soil. While downward flow rates were larger at OBJ2 than at OBJ1 (−3.1 and −0.4 cm/d respectively in Summer 2021; Figure 5), the much larger horizontal flow rates measured in the gravel bed (~150 cm/d, Figure 4a) indicate that the deeper propagation of reducing conditions at OBJ2 likely corresponded to the accumulation of infiltrated solutes from the soil as groundwater underflow traveled along the gravel bed.

3.4. Accumulation of Soil Water Into the Gravel Bed

In the absence of direct measurements of the vertical hydraulic conductivity of the soil, we used the observed accumulation of specific conductance in the gravel bed between wells OBJ1 and OBJ2 to estimate the downward flow rate through the soil/gravel bed interface (Equation 4). We used specific conductance values measured in August 2021, which corresponded to the time period when the horizontal flow velocity in the gravel bed was measured using the point dilution method (Table 1). Additionally, hydraulic gradients and specific conductance were relatively stable over the same time period, suggesting that the system was close to steady state. We assumed that specific conductance was conservative in the gravel bed, and that the mixing height h below the interface with the soil was equal to 2 m, corresponding to the difference of elevation between the interface and the deepest sampling point in the gravel bed at OBJ1 and OBJ2. Details of the calculation are provided in Text S4 of Supporting Information S1. The average downward flow rate between OBJ1 and OBJ2 during August 2021 was then estimated at $q_z = -4.1$ cm/d (Table 1). Using Darcy's law and the average vertical hydraulic gradient at OBJ2, the corresponding vertical hydraulic conductivity of the soil was $K_{s,z} = 1.6 \times 10^{-6}$ m/s, which was lower than the horizontal hydraulic conductivity by one order of magnitude ($K_{s,x} = 1.4 \times 10^{-5}$ m/s, Table 1). This anisotropy is consistent with the heterogeneous, multilayered sediment architecture of the soil observed at the site (Figur S2 in Supporting Information S1) and is typical of depositional floodplain environments (Freeze & Cherry, 1979).

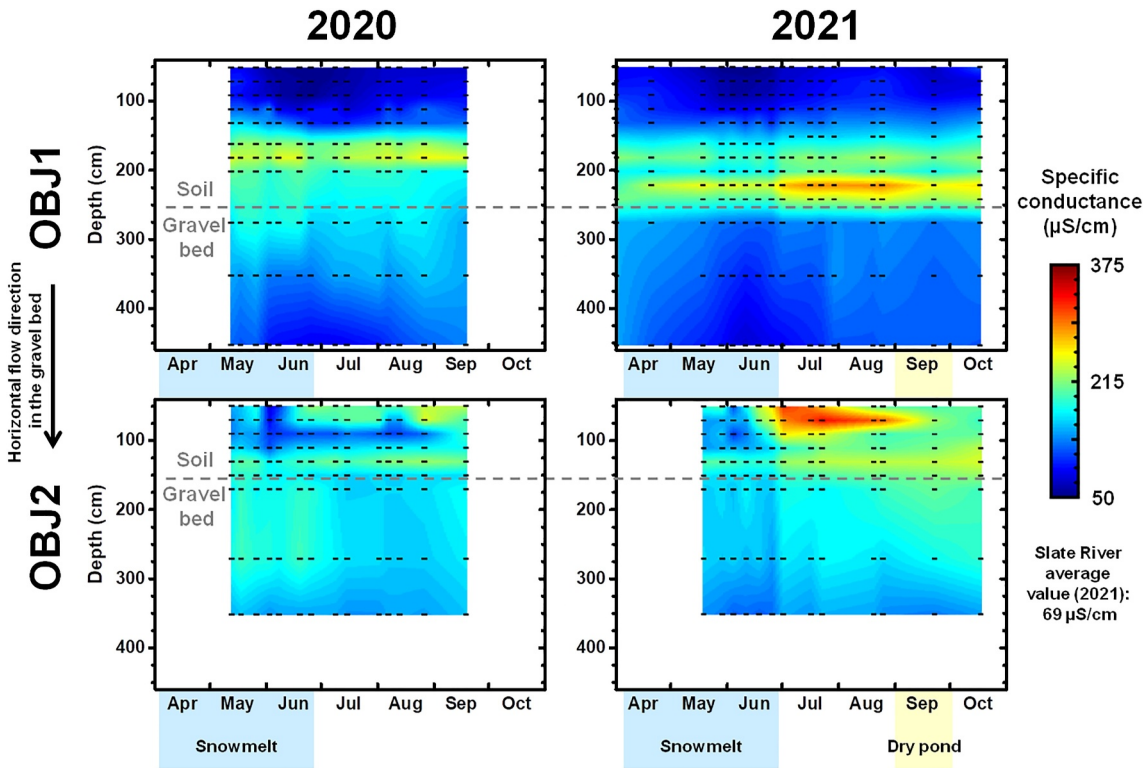

Figure 8. Depth profiles of measured specific conductance in 2020 (left) and 2021 (right) at wells OBJ1 (top) and OBJ2 (bottom). Color contours are based on linear interpolation between concentration measurements denoted by black dots for depth and date. The depth of the soil-gravel bed interface is indicated by the dashed gray line.

To assess the importance of the hydrological connectivity between the soil and the gravel bed, we use the fraction of soil-originated porewater in the gravel bed f_{SW} defined in Equation 5 as the ratio of $q_z x$ (cumulative downward flow from the soil over the lateral travel distance x) over $q_x h$ (cumulative horizontal flow in the gravel bed over the height h). We used the average lateral flow rate measured in the gravel bed (Figure 4a) and the calibrated downward flow rate at OBJ2 (Figure 5). Assuming $x = 50$ m and $h = 10$ m, the fraction of soil-originated water in the gravel bed would represent on average 8% (Figure 10), ranging between 0% (snowmelt or dry pond periods) and 13% (baseflow periods). These variations were mainly driven by variations in vertical flow rates, as horizontal hydraulic gradients in the gravel bed remained mostly stable (Figure 4).

4. Discussion

We monitored groundwater flow and chemical composition in an high-altitude gravel bed river floodplain through representative hydrological transitions, including snowmelt, beaver-induced inundations, and droughts. Results highlighted the importance of the contact between the overlying, fine-grained riparian soil and the underlying gravel valley fill in moderating the water quality response. The floodplain soil modulated the transfer of temporally variable surface drivers (streamflow, beaver pond, droughts) to the hydrologically resilient gravel bed. The soil was further characterized by low DO concentrations, high specific conductance, and high alkalinity, which contrasted markedly with the gravel bed, where groundwater composition was more indicative of in-stream conditions. Hydrological connectivity between the two layers determined the extent of their interaction, and was influenced by surface drivers that altered hydraulic gradients, as well as by geometric considerations such as gravel bed thickness. In particular, inundation due to the presence of a beaver dam increased connectivity and drove the accumulation of anoxic soil porewater in the gravel bed. In the following, we first assess the importance of the hydrological connectivity between the soil and the gravel bed in terms of floodplain groundwater circulation. Based on this analysis, we propose a conceptual model for soil-gravel bed dynamics considering hydrological, geomorphological and biogeochemical drivers. Finally, we discuss the impact of surface water ponding on groundwater within the context of beaver-modified river corridors.

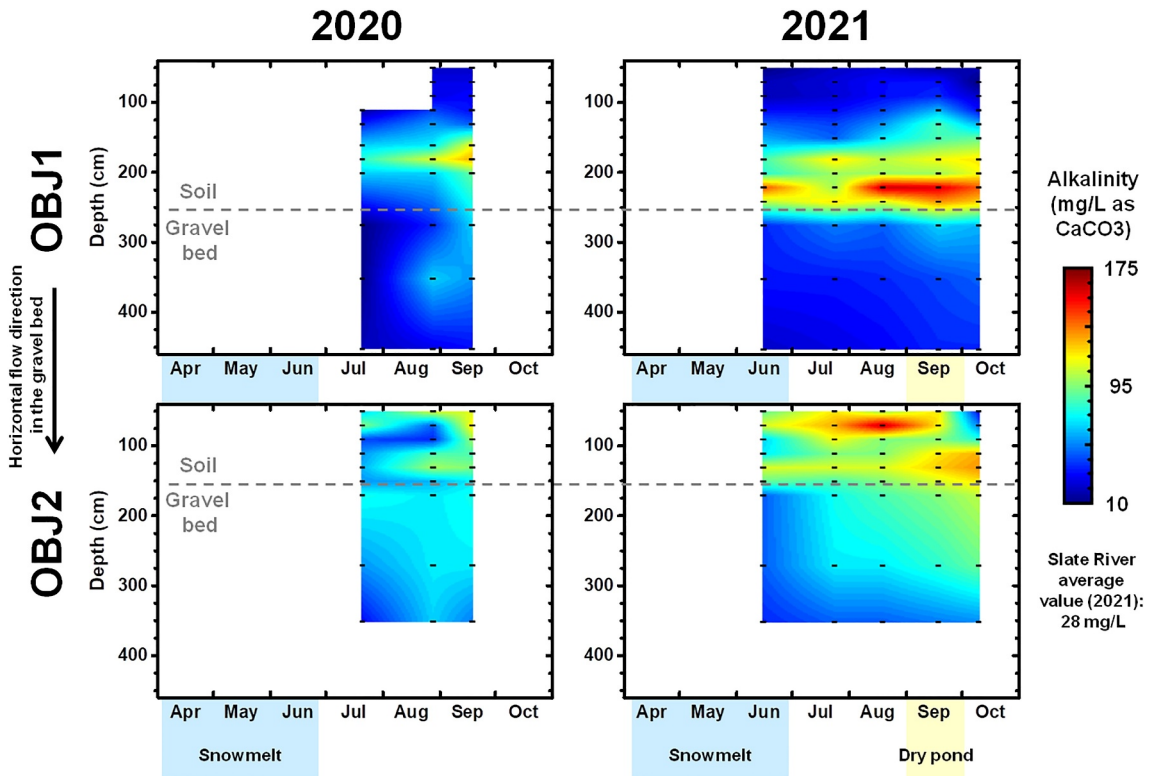

Figure 9. Depth profiles of measured alkalinity in 2020 (left) and 2021 (right) at wells OBJ1 (top) and OBJ2 (bottom). Color contours are based on linear interpolation between concentration measurements denoted by black dots for depth and date. The depth of the soil-gravel bed interface is indicated by the dashed gray line.

4.1. Hydrologic Connectivity in the Floodplain

Our results indicate that hydrological connectivity between the soil and the gravel bed, quantified as the fraction of soil-originated porewater f_{SW}, varies significantly, ranging from 0% during periods of snowmelt or dry ponds to 13% during baseflow (Figure 10). This connectivity was influenced primarily by changes in vertical flow rates, given the stability horizontal hydraulic gradients in the gravel bed. This behavior is bi-modal: connectivity is lowest during both the wettest and driest conditions. The diminished hydrological connectivity during wet periods is surprising and results from an interplay between the hydrological states of the gravel bed and of the beaver pond. During spring snowmelt, hydraulic gradients are diminished and vertical exchange is suppressed due to rising water table in the gravel bed, while during dry pond periods the driver for vertical recharge of the floodplain is absent. Conceptual models often highlight wet periods as important drivers of connectivity (Mahmood et al., 2019). However, for vertically stratified systems, the connectivity of fine-grained, anoxic sediment layers may be greatly diminished, reducing their impact on overall water quality.

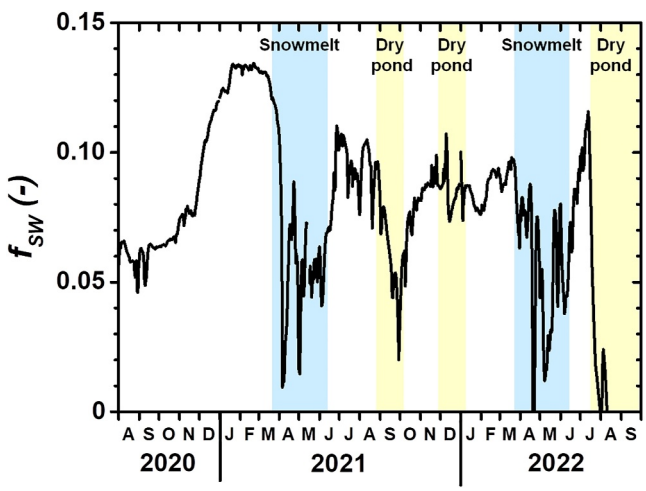

Figure 10. Predicted fraction of soil-originated water f_{SW} accumulated in the gravel bed (Equation 5) at Slate River, for a characteristic horizontal travel distance in the gravel bed x = 50 m and a gravel bed thickness h = 10 m.

Although less biogeochemically active than the soil, the gravel bed can act as a preferential flowpath connecting the floodplain to the stream and, thereby, down-valley areas due to its large hydraulic conductivity. While we did not capture in this study the connectivity between the stream and the gravel bed at the riverbed, it is assumed that these exchanges occur due to topographic and subsurface features, such as inter-meanders flow and lateral hyporheic exchanges (Allgeier et al., 2021; Schmadel et al., 2017). Chemical inputs from the soil zone may thus be transported quickly back to surface water via return

flow. Thus, the gravel bed unit constitutes an important, but often hidden component of floodplain water and elemental budgets, where both connectivity to overlying soils and chemical inputs must be evaluated.

4.2. Linking Hydrologic Connectivity to Water Quality: Solute Convergence Efficiency

The magnitude of hydrologic connectivity quantified by f_{sw} is an important indicator of the potential for soil porewater and solutes to impact groundwater quality in the gravel bed aquifer, especially during inundation events where the hydrological connectivity between the soil and the gravel bed is maximized. Prior experimental studies have pointed to the export of reactive species from fine-grained, anoxic sediments to more conductive zones as an important biogeochemical process in heterogeneous floodplain environments at the sub-meter scale (for example, Aeppli et al., 2022; Babey et al., 2022). Given the potential for elevated inputs and potential retention in the gravel bed, the magnitude of the concentration change in the gravel bed must also be evaluated.

Although the floodplain is inherently a 3-dimensional flow system, our experimental results point to a 1D conceptual model (Equation 3) to describe the accumulation of soil-originated solutes in the gravel bed, mainly due to the stability of the gravel bed flow system (Section 3.1). To link hydrologic connectivity to exported solutes and reactivity, we calculate the SCE (Equation 7), which is a measurement of the speed at which the concentration of a given solute in the gravel bed converges to its concentration in the soil. We first apply the SCE framework to evaluate solute reactivity potential in the gravel bed at the OBJ site. We then use this framework to compare the impact of hydrological transitions at our Slate River site to other gravel bed floodplains in the Upper Colorado River Basin.

4.2.1. Solute Convergence Efficiency at Slate River, CO

Here we explore the extent to which the hydrological connectivity observed at the OBJ site results in exported reactivity from the soil into the gravel bed at the floodplain scale. To this end, we calculate the SCE for specific conductance, alkalinity and DO. As the ratio of vertical to horizontal water flow rates (q_z/q_x) is the same for all solutes between two sampling wells, differences in SCE between solutes can be interpreted as differences in reactivity potential. Using OBJ1 and OBJ2 measurements in August 2021, we find that the SCE for specific conductance and alkalinity were comparable (0.43 and 0.45 respectively, Text S4 in Supporting Information S1), likely due to the substantial contribution of HCO_3^- concentrations to specific conductance (McCleskey et al., 2023). In contrast, the high SCE for DO (0.57) indicates that DO concentrations in the gravel bed decreased due to biogeochemical degradation in addition to mixing with low DO groundwater from the soil. Using $q_z = -4.1$ cm/d (Section 3.4) and Equation 6, we estimated the first order degradation constant for DO in the gravel bed as $k = 9.8 \times 10^{-3} \mathrm{d}^{-1}$ (Text S4 in Supporting Information S1). This degradation rate is similar to other values reported for alluvial aquifers in the literature (Arora et al., 2016; Kolbe et al., 2019; Yabusaki et al., 2017).

Prior work by Dewey et al. (2021) has indicated that anoxic conditions in the fine-grained soil horizons at the OBJ site were associated with high concentrations of dissolved Fe, Mn and organic carbon. DO degradation in the gravel bed could thus result from microbial metabolic activity, potentially stimulated by organic matter exports from the soil, as well as from direct reaction with abiotic reduced solutes (Arora et al., 2016; Babey et al., 2022). These dynamics suggest that exports of reactive solutes from the soil drive the development of a proximal mixing/reaction zone in the gravel bed. This zone is highly sensitive to hydrological changes, as indicated by the fast reoxidation of the gravel bed during snowmelt and dry pond events (Figure 7). These fluctuating redox conditions may impact water quality in several ways. First, reduced metals stored in soils, such as Fe, Mn and As, can be transferred to the gravel bed (Aeppli et al., 2022; Engel et al., 2021; Kumar et al., 2020). Partial reoxidation in the gravel bed may however limit their export to the stream as return flow (Briggs et al., 2019; Dwivedi et al., 2018), although recent work has shown that aqueous phase species in colloidal form (i.e., not truly dissolved) may resist redox transformations (Engel et al., 2023). Second, the accumulation of reduced species (e.g., solid phase FeS) in the gravel bed can reduce and/or immobilize other elements of concern (e.g., NO_3, U, Se) present in the gravel bed due to exchanges with the stream (Ascott et al., 2016; Scott et al., 2014; Sprenger et al., 2011; Yang et al., 2023). However, these immobilized elements might get remobilized during reoxygenation events (Babey et al., 2022). Hydrologic connectivity between soils and gravel beds may thus be an important predictor of "hot moments" for solutes and contaminants often observed in floodplain environments (Lynch et al., 2014).

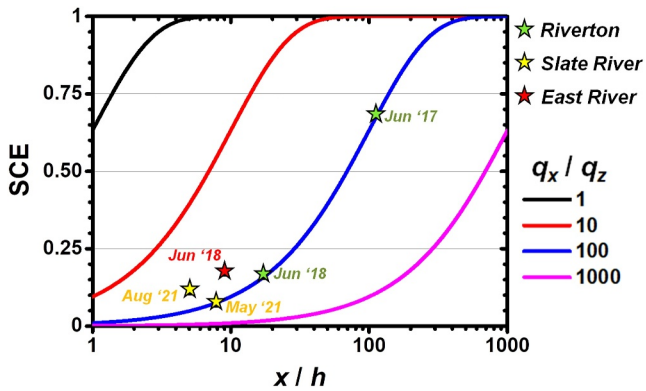

Figure 11. Solute convergence efficiency SCE = $(C(x) - C_0)/(C_s - C_0)$ (Equation 8), as a function of surface flooding width over gravel bed thickness x/h and of the ratio between horizontal and vertical groundwater flow velocity q_x/q_z. SCE was calculated for conservative solutes and for flooding events of various sizes at three Upper Colorado River basin floodplains.

4.2.2. Solute Convergence Efficiency in Montane Floodplains

For a conservative solute, the SCE is a function of geochemical drivers (initial contrast between the concentrations in the soil C_s and in the gravel bed C_0), hydrological drivers (ratio of vertical to lateral flow velocities q_z/q_x) and geomorphological/architectural drivers (gravel bed thickness h and length of connected flowpath x) (Equation 8). Low SCE indicates that the influence of the soil on gravel bed concentrations is minimal, as solute exports from the soil are limited compared to dilution in the gravel bed. We used the SCE framework to compare the impact of hydrological transitions at our Slate River site to other gravel bed floodplains in the Upper Colorado River Basin (Riverton, WY (Dam et al., 2015; Paradis et al., 2022) and East River, CO (Dwivedi et al., 2018; Fox et al., 2021)) where appropriate measurements existed (Figure 11). Details of the calculations are provided in Text S5 in Supporting Information S1. Notably, we assumed that the length of connected flowpath x can be approximated by the width of the corresponding inundation.

For an individual site, hydrological transitions associated with variations in x/h (i.e., greater or smaller inundated area) are predicted to be the primary drivers of exchange efficiency. This is because the vertical and horizontal Darcy flow rates are fairly stable and likely constrained by geomorphology (regional topographic gradient for gravel bed flow, elevation difference between the gravel bed and the pond for soil flow). However, the magnitude of the flooding can vary considerably between snowmelt and baseflow (e.g., Slate River) or between two different hydrological years (e.g., Riverton). For inter-sites comparison, differences in underlying architectures (h, K_z, K_x) will be additional key factors. For instance, thinner gravel bed layers at Riverton ($h \sim 3$ m) and East River ($h \sim 1$ m) compared to Slate River ($h \sim 10$ m) yielded a faster convergence between soil and gravel bed concentrations. Finally, Figure 11 also points to potential consequences of climate change on hydrological connectivity and groundwater quality. Reduced flooded area associated with drought conditions would shift the Upper Colorado River Basin systems to the left side of the figure, where the SCE is lower, with attendant consequences on water quality (Section 4.2.1).

There are several limitations to the SCE framework presented here that could be addressed by future field and modeling studies. Conceptually, the framework assumes that the system reaches hydrological and geochemical steady state, making it unsuitable for quantifying the impact of transient or fast perturbations such as storm events. The SCE framework further assumes that concentrations in the gravel bed are homogeneous over the mixing height h (Equation 1), precluding its application when a characterization of vertical concentration gradients is required, such as simulations of non-linear biogeochemical reactions (for example, Perzan et al., 2021). Experimentally, limitations include the need for paired hydrological and/or biogeochemical measurements (conservative solute) in the soil and in the gravel bed at two different wells (one upgradient, one downgradient) in the floodplain, as well as the need to determine the length of the connected flowpath between the soil and the gravel bed (x). While we used the width of the inundation as a proxy for x, our study showed that the downward recharge zone induced by the presence of the inundation propagated throughout the floodplain beyond the immediately flooded area (>50 m), and that the downward flow rate q_z decreased with increasing distance from the pond.

4.3. Impact of Beaver Ponds on Groundwater Quality

Our results indicate that the beaver pond at Slate River drove a large fraction of soil water into the gravel bed f_{SW}, which was correlated with high SCE. Although floodplain inundation can be driven by a range of factors, including debris flows and intentional human alterations, beaver recolonization is a major driver of ponding in riparian corridors in the Northern hemisphere. The activity of beavers is widely associated with the enhancement of key riparian zone functions (Larsen et al., 2021), including water storage (Westbrook et al., 2006), fire suppression (Fairfax & Whittle, 2020), flood mitigation (Graham et al., 2022), and enhanced biodiversity (Jordan & Fairfax, 2022). Beaver dams may also help mitigate nitrogen loading of surface waters by increasing their connectivity to riparian sediments where nitrate can be reduced (Dewey et al., 2022). However, beavers alter the hydrology of river corridors in complex ways that may change the water balance through increased

evapotranspiration and impact water quality due to increased stream temperatures and metal release (Briggs et al., 2019; Grudzinski et al., 2022). As a result, studies have found mixed results with respect to groundwater (Bobst et al., 2022; Scamardo & Wohl, 2020) and water quality benefits (Połeć & Grzywna, 2023; Stevenson et al., 2022). Conflicting outcomes, especially with respect to water quality, point to the need to connect the underlying drivers of water quality during inundation and how they scale across different riparian corridors.

Although our study was not intended to specifically target the impact of beaver activities, our results reveal several potential impacts on hydrology and water quality. First, the impacts on groundwater are multi-dimensional. In agreement with other studies, we see minimal impacts to the underlying gravel aquifer flow which is largely driven by the topographic gradient (Bobst et al., 2022; Scamardo & Wohl, 2020). The beaver pond does however increase recharge of surface water into the biologically active but low conductivity soil, which may support riparian vegetation (Westbrook et al., 2013). The water quality response is more complex and linked to the high SCE, which expresses the formation of a significant mixing/reaction zone below the soil/gravel bed interface (Section 4.2.1). While ponding during baseflow induces flushing of reduced soil solutes into the gravel bed, their dilution and partial reoxidation would mitigate their export to the stream through return flow, suggesting that the impact of beaver ponding on water quality might be less important in gravel bed floodplains than in non-gravel bed floodplains. In contrast to inundations not resulting from beaver activity, beaver ponds tend to span over extensive areas upstream and downstream of the dam, and to persist over periods of months or years (Westbrook et al., 2006), which would be associated with higher SCE and higher impact on water quality. Finally, the periodic filling and draining of a beaver pond is associated with fluctuating redox conditions in the gravel bed, with notably a potential fast remobilization of immobilized contaminants when the pond dries out. The impact of beaver ponds on groundwater quality would thus be modulated by the sedimentary architecture of the floodplain and in particular by the thickness of the gravel bed, with deep gravel beds being associated with low SCE and large dilution/reoxidation of soil solutes.

5. Conclusion

We monitored the response of water and solute fluxes to hydrological transitions in a high elevation, gravel bed floodplain in the Upper Colorado River Basin. Results indicate that the vertical hydrological connectivity between the biogeochemically active, but low-permeability soil and the low reactivity, but high-permeability gravel bed is key in determining the overall hydro-biogeochemical function of the floodplain. We identified several regimes of connectivity associated with different combinations of hydrological drivers (snowmelt, drought, flooding) that modulate the sink/source behavior of the riparian soil for redox-sensitive species. Notably, the periodic filling of a beaver pond adjacent to the site enhanced the flushing of anoxic, high conductance, high alkalinity porewater from the soil into the gravel bed. While vertical infiltration rates were two orders of magnitude lower than horizontal flow rates in the gravel bed, soil porewater accumulation over the course of groundwater flow under the floodplain resulted in the formation of a two-meter deep suboxic plume in the generally oxic gravel bed. Mass balance calculations further suggested that this plume was redox reactive, promoting oxygen reduction. When the pond dried out during droughts, or when the floodplain became waterlogged during snowmelt, the gravel bed became more oxic due to diminished hydrological connectivity with the soil. We developed a 1D conceptual framework for soil/gravel bed exchanges, or solute exchange efficiency, that links hydrological, biogeochemical and geomorphological drivers. Comparison of our Slate River site with similar floodplains across the Upper Colorado River Basin indicates that although inundation size is the main driver of intra-floodplain variability in solute exchange efficiency, inter-floodplain variability is mostly controlled by differences in floodplain sedimentary architecture, and in particular, the thickness of the gravel bed valley fill. These findings can be used to establish water and elemental budgets in these globally important mountainous ecosystems.

Data Availability Statement

Data sets are publicly available on the ESS-DIVE repository of the U.S. Department of Energy.

- In situ electrochemical and water quality data (Pierce & Bargar, 2021a, 2021b; Pierce & Boye, 2022):
- Water levels, meteorological and soil sensors data (Perzan et al., 2023a, 2023b; Perzan et al., 2022):

Acknowledgments
Funding was provided by the U.S. Department of Energy (DOE) office of Biological and Environmental Research (BER), Climate and Environmental Sciences Division, through its support of the SLAC Floodplain Hydro-Biogeochemistry Science Focus Area (SFA). SSRL and SLAC are supported by the U.S. Department of Energy, Office of Science, Office of Basic Energy Sciences under Contract No DE-AC02-76SF00515. We acknowledge the support of the Rocky Mountain Biological Laboratory, the Crested Butte Land Trust, and the Bureau of Land Management for supporting access to the research sites. The authors acknowledge Drs. Andy Manning and Richard Wanty for their numerous insightful discussions and guidance in selecting biogeochemical data types and sampling modalities. The authors also thank Kamini Singha and the three anonymous reviewers for their helpful comments that improved the quality of the manuscript.

References

Aeppli, M., Babey, T., Engel, M., Lacroix, E. M., Tolar, B. B., Fendorf, S., et al. (2022). Export of organic carbon from reduced fine-grained zones governs biogeochemical reactivity in a simulated aquifer. *Environmental Science & Technology*, *56*(4), 2738–2746. https://doi.org/10.1021/acs.est.1c04664

Allgeier, J., Martin, S., & Cirpka, O. A. (2021). Systematic evaluation of geometry-driven lateral river-groundwater exchange in floodplains. *Water Resources Research*, *57*(8), e2021WR030239. https://doi.org/10.1029/2021wr030239

Arora, B., Spycher, N. F., Steefel, C. I., Molins, S., Bill, M., Conrad, M. E., et al. (2016). Influence of hydrological, biogeochemical and temperature transients on subsurface carbon fluxes in a flood plain environment. *Biogeochemistry*, *127*(2), 367–396. https://doi.org/10.1007/s10533-016-0186-8

Ascott, M. J., Lapworth, D. J., Gooddy, D. C., Sage, R. C., & Karapanos, I. (2016). Impacts of extreme flooding on riverbank filtration water quality. *Science of the Total Environment*, *554–555*, 89–101. https://doi.org/10.1016/j.scitotenv.2016.02.169

Babey, T., Boye, K., Tolar, B., Engel, M., Noël, V., Perzan, Z., et al. (2022). Simulation of anoxic lenses as exporters of reactivity in alluvial aquifer sediments. *Geochimica et Cosmochimica Acta*, *334*, 119–134. https://doi.org/10.1016/j.gca.2022.07.018

Bembenek, A. (2014). *Upper Slate River watershed plan* rep. Crested Butte. 109.

Berens, P. (2009). CircStat: A MATLAB toolbox for circular statistics. *Journal of Statistical Software*, *31*(10), 1–21. https://doi.org/10.18637/jss.v031.i10

Bobst, A. L., Payn, R. A., & Shaw, G. D. (2022). Groundwater-mediated influences of beaver-mimicry stream restoration: A modeling analysis. *Journal of the American Water Resources Association*, *58*(6), 1388–1406. https://doi.org/10.1111/1752-1688.13044

Briggs, M. A., Wang, C., Day-Lewis, F. D., Williams, K. H., Dong, W., & Lane, J. W. (2019). Return flows from beaver ponds enhance floodplain-to-river metals exchange in alluvial mountain catchments. *Science of the Total Environment*, *685*, 357–369. https://doi.org/10.1016/j.scitotenv.2019.05.371

Cardenas, M. B. (2009). A model for lateral hyporheic flow based on valley slope and channel sinuosity. *Water Resources Research*, *45*(1), W01501. https://doi.org/10.1029/2008wr007442

Clow, D. W. (2010). Changes in the timing of snowmelt and streamflow in Colorado: A response to recent warming. *Journal of Climate*, *23*(9), 2293–2306. https://doi.org/10.1175/2009JCLI2951.1

Dam, W. L., Campbell, S., Johnson, R. H., Looney, B. B., Denham, M. E., Eddy-Dilek, C. A., & Babits, S. J. (2015). Refining the site conceptual model at a former uranium mill site in Riverton, Wyoming, USA. *Environmental Earth Sciences*, *74*(10), 7255–7265. https://doi.org/10.1007/s12665-015-4706-y

Dewey, C., Bargar, J., & Fendorf, S. (2021). Porewater lead concentrations limited by particulate organic matter coupled with ephemeral Iron(III) and sulfide phases during redox cycles within contaminated floodplain soils. *Environmental Science & Technology*, *55*(9), 5878–5886. https://doi.org/10.1021/acs.est.0c08162

Dewey, C., Fox, P., Bouskill, N., Dwivedi, D., Nico, P., & Fendorf, S. (2022). Beaver dams overshadow climate extremes in controlling riparian hydrology and water quality. *Nature Communications*, *13*(1), 6509. https://doi.org/10.1038/s41467-022-34022-0

Dwivedi, D., Steefel, C. I., Arora, B., Newcomer, M., Moulton, J. D., Dafflon, B., et al. (2018). Geochemical exports to river from the intra-meander hyporheic zone under transient hydrologic conditions: East river mountainous watershed, Colorado. *Water Resources Research*, *54*(10), 8456–8477. https://doi.org/10.1029/2018wr023377

Engel, M., Boye, K., Noël, V., Babey, T., Bargar, J. R., & Fendorf, S. (2021). Simulated aquifer heterogeneity leads to enhanced attenuation and multiple retention processes of zinc. *Environmental Science & Technology*, *55*(5), 2939–2948. https://doi.org/10.1021/acs.est.0c06750

Engel, M., Noël, V., Pierce, S., Kovarik, L., Kukkadapu, R. K., Pacheco, J. S. L., et al. (2023). Structure and composition of natural Ferrihydrite Nano-colloids in anoxic groundwater. *Water Research*, *238*, 119990. https://doi.org/10.1016/j.watres.2023.119990

Fairfax, E., & Whittle, A. (2020). Smokey the beaver: Beaver-dammed riparian corridors stay green during wildfire throughout the Western United States. *Ecological Applications*, *30*(8), e02225. https://doi.org/10.1002/eap.2225

Fetter, C. W. (1981). Determination of the direction of groundwater flow. *Groundwater Monitoring & Remediation*, *1*(3), 28–31. https://doi.org/10.1111/j.1745-6592.1981.tb00813.x

Fox, P., Anderson, C., Keiluweit, M., Dewey, C., & Nico, P. (2021). 2018 meander C floodplain groundwater chemistry from the East River watershed, Colorado [Dataset]. *Watershed Function SFA, ESS-DIVE Repository*. https://doi.org/10.15485/1836833

Freeze, A., & Cherry, J. (1979). *Groundwater*. Prentice Hall.

Gaskill, D. L., Godwin, L. H., & Mutschler, F. E. (1967). Geologic map of the Oh-Be-joyful quadrangle, report rep. *578*. https://doi.org/10.3133/gq578

Graham, H. A., Puttock, A. K., Elliott, M., Anderson, K., & Brazier, R. E. (2022). Exploring the dynamics of flow attenuation at a beaver dam sequence. *Hydrological Processes*, *36*(11), e14735. https://doi.org/10.1002/hyp.14735

Grudzinski, B. P., Fritz, K., Golden, H. E., Newcomer-Johnson, T. A., Rech, J. A., Levy, J., et al. (2022). A global review of beaver dam impacts: Stream conservation implications across biomes. *Global Ecology and Conservation*, *37*, e02163. https://doi.org/10.1016/j.gecco.2022.e02163

Hatfield, K., Annable, M., Cho, J., Rao, P. S. C., & Klammler, H. (2004). A direct passive method for measuring water and contaminant fluxes in porous media. *Journal of Contaminant Hydrology*, *75*(3), 155–181. https://doi.org/10.1016/j.jconhyd.2004.06.005

Hauer, F. R., Locke, H., Dreitz, V. J., Hebblewhite, M., Lowe, W. H., Muhlfeld, C. C., et al. (2016). Gravel-bed river floodplains are the ecological nexus of glaciated mountain landscapes. *Science Advances*, *2*(6), e1600026. https://doi.org/10.1126/sciadv.1600026

Hidalgo, H. G., Das, T., Dettinger, M. D., Cayan, D. R., Pierce, D. W., Barnett, T. P., et al. (2009). Detection and attribution of streamflow timing changes to climate change in the Western United States. *Journal of Climate*, *22*(13), 3838–3855. https://doi.org/10.1175/2009JCLI2470.1

Hoppe, J. (2013). *Geochemical characterization and longevity estimates of a permeable reactive barrier system remediating a 90Sr plume*. UWSpace.

Janot, N., Lezama Pacheco, J. S., Pham, D. Q., O'Brien, T. M., Hausladen, D., Noël, V., et al. (2016). Physico-chemical heterogeneity of organic-rich sediments in the rifle aquifer, CO: Impact on uranium biogeochemistry. *Environmental Science & Technology*, *50*(1), 46–53. https://doi.org/10.1021/acs.est.5b03208

Jordan, C. E., & Fairfax, E. (2022). Beaver: The North American freshwater climate action plan. *Wiley Interdisciplinary Reviews-Water*, *9*(4), e1592. https://doi.org/10.1002/wat2.1592

Käser, D., & Hunkeler, D. (2016). Contribution of alluvial groundwater to the outflow of mountainous catchments. *Water Resources Research*, *52*(2), 680–697. https://doi.org/10.1002/2014WR016730

Kimball, B. A., Runkel, R. L., Wanty, R. B., & Verplanck, P. L. (2010). Reactive solute-transport simulation of pre-mining metal concentrations in mine-impacted catchments: Redwell Basin, Colorado, USA. *Chemical Geology*, *269*(1), 124–136. https://doi.org/10.1016/j.chemgeo.2009.05.024

Kolbe, T., de Dreuzy, J. R., Abbott, B. W., Aquilina, L., Babey, T., Green, C. T., et al. (2019). Stratification of reactivity determines nitrate removal in groundwater. *Proceedings of the National Academy of Sciences*, *116*(7), 2494–2499. https://doi.org/10.1073/pnas.1816892116

Kumar, N., Noël, V., Planer-Friedrich, B., Besold, J., Lezama-Pacheco, J., Bargar, J. R., et al. (2020). Redox heterogeneities promote Thioarsenate formation and release into groundwater from low arsenic sediments. *Environmental Science & Technology*, *54*(6), 3237–3244. https://doi.org/10.1021/acs.est.9b06502

Larsen, A., Larsen, J. R., & Lane, S. N. (2021). Dam builders and their works: Beaver influences on the structure and function of river corridor hydrology, geomorphology, biogeochemistry and ecosystems. *Earth-Science Reviews*, *218*, 103623. https://doi.org/10.1016/j.earscirev.2021.103623

Lide, D. R. (2004). *CRC handbook of chemistry and physics* (84th ed.), CRC Press LLC. 2616.

Lynch, S. F. L., Batty, L. C., & Byrne, P. (2014). Environmental risk of metal mining contaminated river bank sediment at redox-transitional zones. *Minerals*, *4*(1), 52–73. https://doi.org/10.3390/min4010052

Mahmood, M. N., Schmidt, C., Fleckenstein, J. H., & Trauth, N. (2019). Modeling the impact of stream discharge events on riparian solute dynamics. *Groundwater*, *57*(1), 140–152. https://doi.org/10.1111/gwat.12664

Manning, A. H., Verplanck, P. L., Caine, J. S., & Todd, A. S. (2013). Links between climate change, water-table depth, and water chemistry in a mineralized mountain watershed. *Applied Geochemistry*, *37*, 64–78. https://doi.org/10.1016/j.apgeochem.2013.07.002

McCleskey, R. B., Cravotta, C. A., Miller, M. P., Tillman, F., Stackelberg, P., Knierim, K. J., & Wise, D. R. (2023). Salinity and total dissolved solids measurements for natural waters: An overview and a new salinity method based on specific conductance and water type. *Applied Geochemistry*, *154*, 105684. https://doi.org/10.1016/j.apgeochem.2023.105684

Meixner, T., Manning, A. H., Stonestrom, D. A., Allen, D. M., Ajami, H., Blasch, K. W., et al. (2016). Implications of projected climate change for groundwater recharge in the Western United States. *Journal of Hydrology*, *534*, 124–138. https://doi.org/10.1016/j.jhydrol.2015.12.027

Miller, M. P., Buto, S. G., Susong, D. D., & Rumsey, C. (2016). The importance of base flow in sustaining surface water flow in the Upper Colorado River Basin. *Water Resources Research*, *52*(5), 3547–3562. https://doi.org/10.1002/2015WR017963

Mishra, A., Alnahit, A., & Campbell, B. (2021). Impact of land uses, drought, flood, wildfire, and cascading events on water quality and microbial communities: A review and analysis. *Journal of Hydrology*, *596*, 125707. https://doi.org/10.1016/j.jhydrol.2020.125707

Nazaroff, W. W., & Alvarez-Cohen, L. (2001). *Environmental engineering science*. John Wiley & Sons Incorporated.

Noël, V., Boye, K., Kukkadapu, R. K., Bone, S., Lezama Pacheco, J. S., Cardarelli, E., et al. (2017). Understanding controls on redox processes in floodplain sediments of the Upper Colorado River Basin. *Science of the Total Environment*, *603–604*, 663–675. https://doi.org/10.1016/j.scitotenv.2017.01.109

Pan, D., Williams, K. H., Robbins, M. J., & Weber, K. A. (2018). Uranium retention in a bioreduced region of an alluvial aquifer induced by the influx of dissolved oxygen. *Environmental Science & Technology*, *52*(15), 8133–8145. https://doi.org/10.1021/acs.est.8b00903

Paradis, C., Van Ee, N., Hoss, K., Meurer, C., Tigar, A., Reimus, P., & Johnson, R. (2022). Single-well injection-drift test to estimate groundwater velocity. *Groundwater*, *60*(4), 565–570. https://doi.org/10.1111/gwat.13184

Perzan, Z., Babey, T., Caers, J., Bargar, J. R., & Maher, K. (2021). Local and global sensitivity analysis of a reactive transport model simulating floodplain redox cycling. *Water Resources Research*, *57*(12), e2021WR029723. https://doi.org/10.1029/2021WR029723

Perzan, Z., & Chapin, T. (2023). WellSTIC: A cost-effective sensor for performing point dilution tests to measure groundwater velocity in shallow aquifers. *Water Resources Research*, *59*(1), e2022WR033223. https://doi.org/10.1029/2022WR033223

Perzan, Z., Maher, K., Boye, K., & Bargar, J. R. (2023a). Meteorological, reference evapotranspiration and estimated transpiration data, July 2020–Dec 2021, Slate River floodplain, Crested Butte, Colorado [Dataset]. *Groundwater Quality SFASESS-DIVE Repository*. https://doi.org/10.15485/1958211

Perzan, Z., Maher, K., Boye, K., & Bargar, J. R. (2023b). Soil water content, matric potential, carbon dioxide and oxygen concentrations [Dataset]. *Oct 2018–Dec 2021, Slate River Floodplain, Crested Butte, Colorado. Groundwater Quality SFA, ESS-DIVE Repository*. https://doi.org/10.15485/1958210

Perzan, Z., Pierce, S., & Boye, K. (2022). Groundwater level elevation and temperature data, Oct 2018–Dec 2021 [Dataset]. *Slate River Floodplain, Crested Butte, CO. Groundwater Quality SFA, ESS-DIVE Repository*. https://doi.org/10.15485/1908248

Pierce, S., & Bargar, J. R. (2021a). Specific conductivity, pH, dissolved oxygen, water temperature and alkalinity in situ data; Slate River floodplain, Crested Butte, CO; March 2021–October 2021 [Dataset]. *Groundwater Quality SFA, ESS-DIVE Repository*. https://doi.org/10.15485/1829500

Pierce, S., & Bargar, J. R. (2021b). Specific conductivity, pH, dissolved oxygen, water temperature, alkalinity and sulfide in-situ data; Slate River floodplain, Crested Butte, CO; May 2020-October 2020 [Dataset]. *Groundwater Quality SFA, ESS-DIVE Repository*. https://doi.org/10.15485/1813302

Pierce, S., & Boye, K. (2022). In situ electrochemical and water quality data; Slate River and East River floodplains, Crested Butte, CO; May 2022–September 2022 [Dataset]. *Groundwater Quality SFA, ESS-DIVE Repository*. https://doi.org/10.15485/1896309

Połeć, K., & Grzywna, A. (2023). Influence of natural barriers on small rivers for changes in water quality Parameters. *Water*, *15*(11), 2065. https://doi.org/10.3390/w15112065

Rumsey, C. A., Miller, M. P., Susong, D. D., Tillman, F. D., & Anning, D. W. (2015). Regional scale estimates of baseflow and factors influencing baseflow in the Upper Colorado River Basin. *Journal of Hydrology: Regional Studies*, *4*, 91–107. https://doi.org/10.1016/j.ejrh.2015.04.008

Scamardo, J., & Wohl, E. (2020). Sediment storage and shallow groundwater response to beaver dam analogues in the Colorado Front Range, USA. *River Research and Applications*, *36*(3), 398–409. https://doi.org/10.1002/rra.3592

Schmadel, N. M., Ward, A. S., & Wondzell, S. M. (2017). Hydrologic controls on hyporheic exchange in a headwater mountain stream. *Water Resources Research*, *53*(7), 6260–6278. https://doi.org/10.1002/2017wr020576

Scott, D. T., Keim, R. F., Edwards, B. L., Jones, C. N., & Kroes, D. E. (2014). Floodplain biogeochemical processing of floodwaters in the Atchafalaya River Basin during the Mississippi river flood of 2011. *Journal of Geophysical Research: Biogeosciences*, *119*(4), 537–546. https://doi.org/10.1002/2013JG002477

Sprenger, C., Lorenzen, G., Hülshoff, I., Grützmacher, G., Ronghang, M., & Pekdeger, A. (2011). Vulnerability of bank filtration systems to climate change. *Science of the Total Environment*, *409*(4), 655–663. https://doi.org/10.1016/j.scitotenv.2010.11.002

Stanford, J. A., & Ward, J. V. (1993). An ecosystem perspective of alluvial rivers: Connectivity and the hyporheic corridor. *Journal of the North American Benthological Society*, *12*(1), 48–60. https://doi.org/10.2307/1467685

Stevenson, J. R., Dunham, J. B., Wondzell, S. M., & Taylor, J. (2022). Dammed water quality—Longitudinal stream responses below beaver ponds in the Umpqua River Basin, Oregon. *Ecohydrology*, *15*(4), e2430. https://doi.org/10.1002/eco.2430

Todd, A. S., Manning, A. H., Verplanck, P. L., Crouch, C., McKnight, D. M., & Dunham, R. (2012). Climate-change-driven deterioration of water quality in a mineralized watershed. *Environmental Science & Technology*, *46*(17), 9324–9332. https://doi.org/10.1021/es3020056

Tolar, B. B., Boye, K., Bobb, C., Maher, K., Bargar, J. R., & Francis, C. A. (2020). Stability of floodplain subsurface microbial communities through seasonal hydrological and geochemical cycles. *Frontiers in Earth Science*, *8*, 338. https://doi.org/10.3389/feart.2020.00338

Udall, B., & Overpeck, J. (2017). The twenty-first century Colorado River hot drought and implications for the future. *Water Resources Research*, *53*(3), 2404–2418. https://doi.org/10.1002/2016WR019638

Voltz, T., Gooseff, M., Ward, A. S., Singha, K., Fitzgerald, M., & Wagener, T. (2013). Riparian hydraulic gradient and stream-groundwater exchange dynamics in steep headwater valleys. *Journal of Geophysical Research: Earth Surface*, *118*(2), 953–969. https://doi.org/10.1002/jgrf.20074

Wang, C., Gomez-Velez, J. D., & Wilson, J. L. (2018). The importance of capturing topographic features for modeling groundwater flow and transport in mountainous watersheds. *Water Resources Research*, *54*(12), 10313–10338. https://doi.org/10.1029/2018WR023863

Ward, A. S., Schmadel, N. M., Wondzell, S. M., Harman, C., Gooseff, M. N., & Singha, K. (2016). Hydrogeomorphic controls on hyporheic and riparian transport in two headwater mountain streams during base flow recession. *Water Resources Research*, *52*(2), 1479–1497. https://doi.org/10.1002/2015WR018225

Westbrook, C. J., Cooper, D. J., & Baker, B. W. (2006). Beaver dams and overbank floods influence groundwater–surface water interactions of a Rocky Mountain riparian area. *Water Resources Research*, *42*(6), W06404. https://doi.org/10.1029/2005WR004560

Westbrook, C. J., Cooper, D. J., & Butler, D. R. (2013). 12.20 beaver hydrology and geomorphology. In J. F. Shroder (Ed.), *Treatise on geomorphology* (pp. 293–306). Academic Press. https://doi.org/10.1016/B978-0-12-374739-6.00337-7

Yabusaki, S. B., Wilkins, M. J., Fang, Y., Williams, K. H., Arora, B., Bargar, J., et al. (2017). Water table dynamics and biogeochemical cycling in a shallow, variably-saturated floodplain. *Environmental Science & Technology*, *51*(6), 3307–3317. https://doi.org/10.1021/acs.est.6b04873

Yang, F., Yue, S., Wu, X., Zhang, C., Li, D., & Zhu, R. (2023). Effects of flood inundation on biogeochemical processes in groundwater during riverbank filtration. *Journal of Hydrology*, *617*, 129101. https://doi.org/10.1016/j.jhydrol.2023.129101

References From the Supporting Information

Dewey, C., Fendorf, S., Francis, C., & Nico, P. (2020). *Water quality in dynamic redox environments: Coupled hydrologic-biogeochemical controls on metal contaminant mobility*. Ph.D Thesis. Stanford University. Retrieved from https://www.proquest.com/openview/3b9c4032f14194bf517011ba0e3400db/1?pq-origsite=gscholar&cbl=44156

DOE. (2013). 2012 enhanced characterization & monitoring report, Riverton, Wyoming, processing site rep, 53.

DOE. (2019). Three years of multilevel monitoring data at the Riverton, Wyoming, processing site that show contaminant increases after river flooding events and a large recharge event *rep*.48.

Looney, B. B., Denham, M. E., & Eddy-Dilek, C. A. (2014). Independent technical evaluation and recommendations for contaminated groundwater at the department of energy office of legacy management Riverton processing site*Rep*, medium: ED; size.79.